Vacancy defect complexes in silicon: Charges and spin order

Yu Liu,[1] Ruiqun Pan,[2] Xinghong Zhang,[3] Jiecai Han,[3] Quan Yuan,[3] Ying Tian,[4] Ye Yuan,[1,5] Fang Liu,[1,5] Yutian Wang,[1] Alpha T. N'Diaye,[6] Elke Arenholz,[6] Xiaolong Chen,[4] Young Sun,[4] Bo Song,[7,*] and Shengqiang Zhou[1]

[1]*Helmholtz-Zentrum Dresden-Rossendorf, Institute of Ion Beam Physics and Materials Research, 01328 Dresden, Germany*

[2]*Changchun University of Science and Technology, Changchun 130022, China*

[3]*Centre for Composite Materials and Structure, Harbin Institute of Technology, Harbin 150080, China*

[4]*Institute of Physics, Chinese Academy of Sciences, Beijing 100190, China*

[5]*Technische Universität Dresden, 01062 Dresden, Germany*

[6]*Advanced Light Source, Lawrence Berkeley National Laboratory, Berkeley, California 94720, USA*

[7]*Academy of Fundamental and Interdisciplinary Sciences, Harbin Institute of Technology, Harbin 150080, China*

(Received 27 April 2016; revised manuscript received 24 August 2016; published 14 November 2016)

We investigate the interaction between charges and spin order of the defect complex V6 in silicon. The first-principles calculations predict spin resolved band splitting incurred by a neutral V6 yet with no net spin. Therefore, any shift of Fermi level can trigger the spin polarization. Both *s* and *p* states contribute local moments in the positively charged V6. The ferromagnetic coupling is only obtained between a positively charged V6 and a neutral one. In silicon after neutron irradiation, magnetism is achieved even at room temperature. The $3s^*3p^*$ hybrid states of V6 are probably responsible for the observed long-range magnetic order. Our results unravel the role of charged V6 in inducing magnetism and will be useful in understanding and further manipulating the intrinsic properties of defect complexes in silicon and other semiconductors.

DOI: 10.1103/PhysRevB.94.195204

As is well known, the integrated circuit has profoundly affected all aspects of human beings, which makes silicon a shining superstar among materials. In the silicon-based integrated circuits, high carrier concentrations ($n_e > 10^{20}\,\mathrm{cm}^{-3}$) are required to provide a sufficient conductance in both the drain and source areas [1]. One essential step in state-of-the-art technologies to realize this aim is usually achieved by doping or by ion implantation. Thus, the lattice defects of various kinds produced in this process are unavoidable. Among lattice defects, defect complexes are particularly striking due to their variability and complexity. First-principles calculations have predicted that forming D3V or D4V (D: donor, V: vacancy) defects is exothermic [2] while forming DV or D2V is endothermic [3]. They have been investigated experimentally by combining positron lifetime, electron momentum distribution measurements [4], and atomic-scale imaging [5] to understand their electrical deactivation. Their formation mechanism has further been explored by kinetic migration processes [6]. Then, the formation of DV or D2V in highly Sb-doped silicon films has been studied by both theoretical calculations and experimental characterizations [7]. The stability of dopant-pair defects in boron- and phosphorus-doped silicon nanowires has also been investigated [8]. V6 of hexagonal ring constituted by six silicon single vacancies has been revealed to be remarkably stable, electrically inactive, virtually invisible, and barely distorted, which often appears in irradiated or ion implanted silicon [9,10]. Donor pair (DP) of two donors without vacancy [11] as well as donor-pair-vacancy-interstitial complexes [12] in highly *n*-doped silicon has also been proposed.

The structural and energetic information along with the electrical deactivation of these complexes has been well clarified. However, further investigation is still needed to fully understand the influence of such intrinsic complexes on the fundamental properties of silicon, such as, the magnetism. Understanding the properties in silicon due to these lattice defects is not only of great importance in evaluating the effects on the materials' and devices' performance, but the exploration of their potential applications is also expected. Herein we theoretically predict and then experimentally verify the interaction between charges and spin order of the V6 in silicon. We employ first-principles calculations and demonstrate that the neutral V6 has no net spin while any shift of Fermi level can conduce to the spin polarization due to band splitting. Around a positively charged V6, both *s* and *p* states of nearest-neighbor silicon atoms are involved donating most of the magnetic moments. The coupling between two positively charged V6s is antiferromagnetic (AFM) while the ferromagnetic (FM) coupling is achieved when V6s are partially positively charged. The predictions are experimentally verified in silicon after neutron irradiation. Magnetism can still be obtained at room temperature (RT). The V6 concentration derived from the predicted local moment value and magnetization is consistent with that obtained from the measurements. The $3s^*3p^*$ hybrid states of slightly positively charged V6 are assigned to be responsible for the observed magnetism.

In Fig. 1(a) we calculated the density of phonon states (DOPS). It confirms the dynamic stability of V6, as all its phonon branches acquire positive frequencies and no imaginary modes can be observed [13]. It is well consistent with previous results in which it has been proved to be both energetically and dynamically favored [9,10]. Figure 1(b) shows that several extra energy bands emerge in the band gap due to V6 appearance. The energies between bands are relatively small, which makes V6 a candidate in the study of qubit [14]. Band splitting is found due to spin polarization in the electronic structure, while the net spin is

*songbo@hit.edu.cn

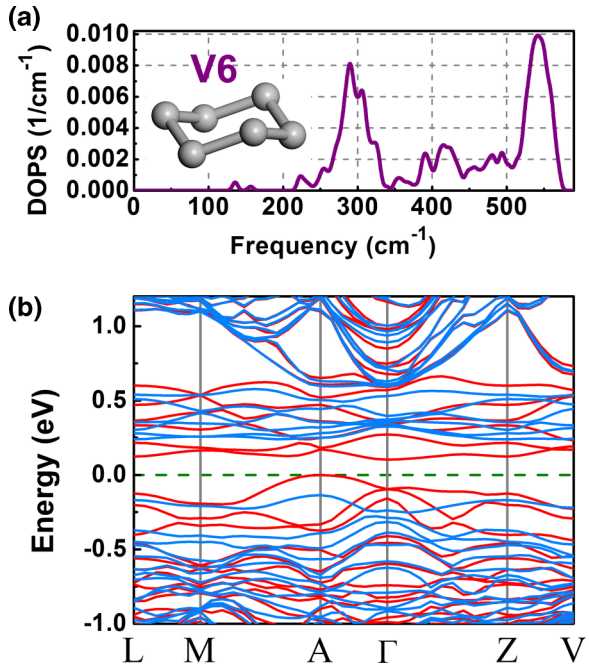

FIG. 1. The DOPS (a) and the band structure (b) of a 144-atom silicon supercell with a neutral V6. The inset shows the structure of V6. The majority spin shows in pink and the minority in blue.

nearly zero ($0.007\,\mu_B$). It is implied that the spin states are occasionally fully occupied. If the Fermi level is shifted, the spin polarization could be revealed.

We alter the charge number of the supercell to check this effect. The difference of energy between spin-polarized states and spin-unpolarized ones, coined as spin-polarization energy, is estimated to be 11 meV for positively charged $V6^+$. The calculated spin-resolved density of states (DOS) [see Fig. 2(a)] manifests that each $V6^+$ yields a magnetic moment of $\sim 0.56\,\mu_B$. The spin polarization between the minority-spin and majority-spin states induced by $V6^+$ incurs a 104 meV splitting. The partial DOS shows that the local moments near the Fermi level mainly originate from p states as shown in Fig. 2(b). Different from the previous understanding [15,16], some s states are also involved in the formation of the moments around the bottom of the conduction band. This could be understood as that the sp^3 bonding orbitals almost remain intact because the distortion brought by V6 is rather weak [9,10].

Figure 3(a) displays the charge density isosurface for the 144-atom silicon supercell with a $V6^+$. It indicates that the magnetic moments are mostly brought by the nearest-neighbor silicon atoms of $V6^+$. Similar calculated results have been obtained in vacancy-including carbides [17] and nitrides [18]. However, in this case, the spin for half of the nearest-neighbor silicon atoms (6 out of 12) is up and the rest is down. Figures 3(b) and 3(c) provide a manifestation that the value of up spin on each atom is larger than that of down spin, which is similar to the ferrimagnetic order. This can be attributed to the increase of the nearest-neighbor atoms and the influence to the symmetry due to the complexity of V6. In the current area of defect-induced magnetism, the behavior of $V6^+$ is unique and representative.

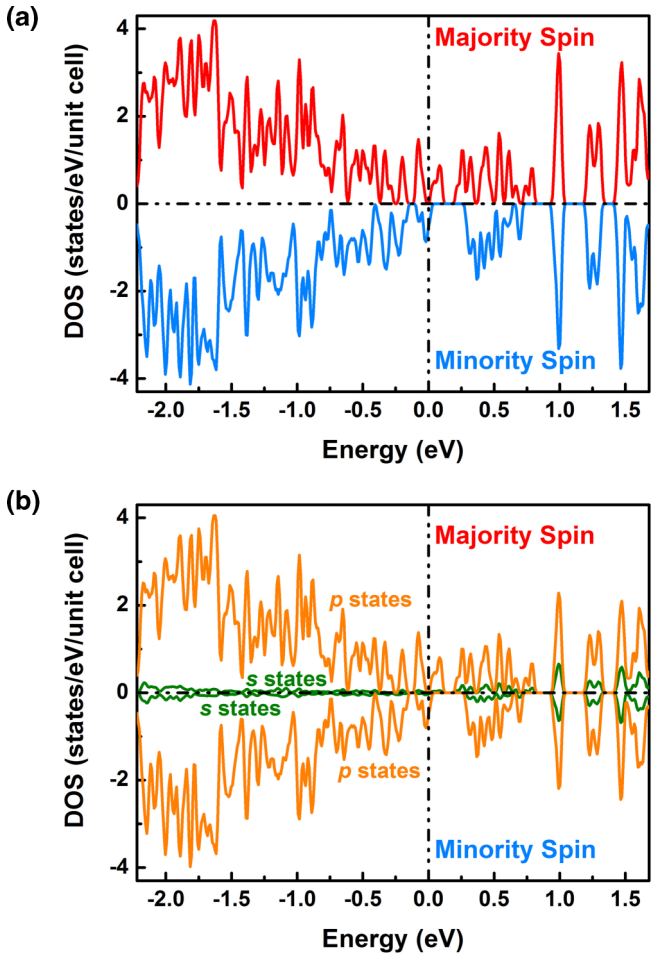

FIG. 2. Total (a) and partial (b) spin-resolved DOS of a 144-atom silicon supercell with a $V6^+$.

Another supercell was built by putting two 144-atom supercells side by side to investigate the coupling (FM or AFM) between the local moments of $V6^+$. With the nearest-neighbor Heisenberg model, the coupling strength can be gained via the energy difference between the AFM and FM phases $E_{\mathrm{AFM}ab} - E_{\mathrm{FM}} = 4J_{ab}S^2$ and $E_{\mathrm{AFM}c} - E_{\mathrm{FM}} = 4J_cS^2$, in which E_{FM}, $E_{\mathrm{AFM}ab}$, and $E_{\mathrm{AFM}c}$ are the total energies of FM, AFM in a-b plane and AFM along c axis configurations, respectively; J_{ab} and J_c are designated for the nearest-neighbor exchange interaction in and out of a-b plane, while S is assigned to represent the net spin originated from defects, $0.56\,\mu_B$ per V6 in this case. A negative J indicates that the coupling is AFM or otherwise FM. The magnetic configuration of $V6^+$s is checkerboard antiferromagnetism with J_{ab} of -14.6 meV and J_c of 55.5 meV, respectively. We further consider the situation of partially positively charged V6s. The equivalent spin-polarization energy is largely increased from 11 to around 37 meV, which manifests the spin-polarized state stable above RT. The exchange interactions J_{ab} and J_c are 238 and 224 meV, so partially charged V6 favors the FM ordering. The previous works have indicated that the V6 defect is electrically inactive [9,10]. No net spin emerges in the neutral V6, while the charged ones are spin polarized but not easily obtained. If

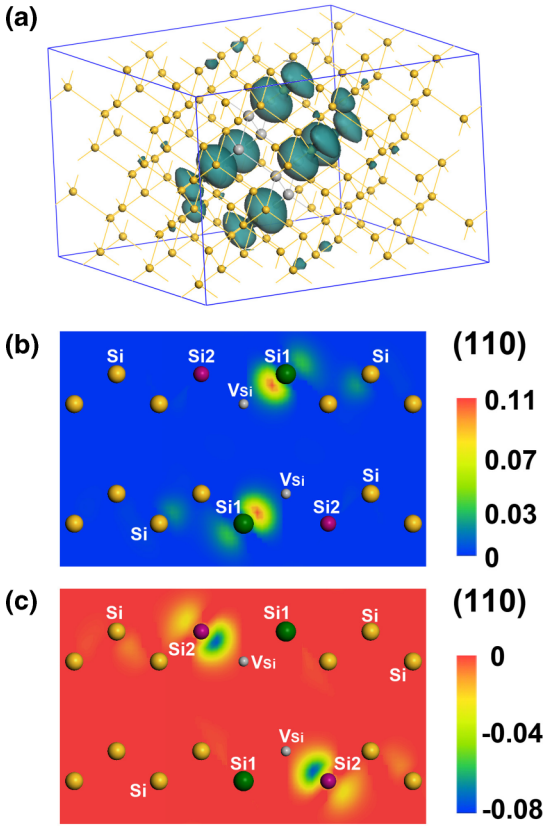

FIG. 3. (a) Spin resolved isosurface charge density plot in dark green of a 144-atom silicon supercell with a $V6^{+}$ (isovalue is 0.01 $e/\text{Å}^3$), demonstrating both the localized and the extended states due to the defect. (b) and (c) Isosurface charge density slices across two vacancies in V6 and four of its nearest-neighbor silicon atoms on (110) to show the up spin (b) and down spin (c) distribution. Legend is in unit of $e/\text{Å}^3$. Non-nearest neighbor, the first class nearest neighbor and the second class nearest neighbor silicon atoms are shown in yellow (Si), green (Si1), purple (Si2), and vacancy sites (V_{Si}) in gray, respectively.

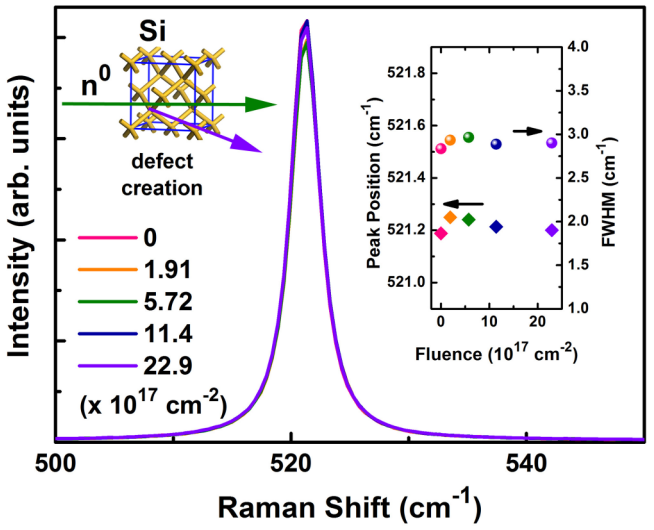

FIG. 4. Raman spectra for the irradiated and pristine silicon. Left inset: Schematic illustration of neutron irradiating silicon process. Right inset: The peak position and FWHM dependence of neutron irradiation fluence.

only partially charging is required, the expected magnetism is possibly achieved.

Silicon after neutron irradiation (as illustrated in the left inset of Fig. 4) provides a well-defined system to induce V6s and verify the predictions from the first-principles calculations [19]. After neutron irradiation, the crystal structure of the irradiated silicon samples was characterized by using Raman spectroscopy demonstrated in Fig. 4. The Raman spectra for irradiated silicon with varying fluences are almost coincident with that of the pristine one, indicating that the lattice is not significantly damaged. More details in the right inset of Fig. 4, in which the peak position (left axis) and full width at half maximum (FWHM, right axis) as a function of the irradiation fluence, yet cannot provide the evidence to prove the possible damage induced by irradiation. The explanation may lay on the relatively small scattering cross section of silicon to neutron, which may lower the efficiency of neutrons to create defects [20]. As Raman merely detects the signal from the surface, another possibility is that defects only distribute in the bulk.

To probe the defect types and concentrations, positron annihilation lifetime spectroscopy measurements on irradiated silicon pieces were carried out. It is well accepted that it is a useful nondestructive experimental technique to gain information about the defects in solid state materials with ppm-level detection sensitivity [21–23]. Herein a sandwiched structure of the sample-source-sample in the form as "as-irradiated silicon wafer/^{22}Na source/as-irradiated silicon wafer" (the initial maximum energy of positrons is about 0.54 MeV) was utilized in a fast-slow coincidence ORTEC system with a time resolution of ∼195 ps. To minimize the influence of the statistical error during the measurement of lifetimes, more than two million counts were gathered for each spectrum. Owing to the various annihilation sites, single lifetime spectrum can be considered as a linear combination of the exponential functions. Generally, as-measured lifetime spectra could be fitted into three exponential functions, representing three types of annihilation sites, respectively. Then, we deconvoluted and fit the lifetime spectra by using the program (LT-9) according to this rule [24]. After fitting, the ∼2 ns long lifetime (τ_3) corresponding to annihilations at sample surface or voids is very small in its fraction and will be ignored in the following analysis.

Two fitted positron lifetimes τ_1 and τ_2 and a component I_2 corresponding to the fraction of the longer lifetime (τ_2) as a function of the neutron irradiation fluence are shown in Fig. 5. The lifetime τ_1 is 162 ± 8 ps, usually attributed to the bulk, similar to that of the deformed silicon (∼160 ps) [25]. The lifetime τ_2, taking a value of 378 ± 33 ps, independent of irradiation fluence, is assigned to V6 [26]. Further information about the relative concentration of the defects can be gained from the component I_2, which was found to be closely associated with the neutron irradiation fluence. So the concentration of V6 increases with neutron fluence increasing.

In the pristine silicon sample, only the diamagnetic signal was obtained, while in low magnetic field range a minor hysteresis loop could be observed in series of the irradiated silicon

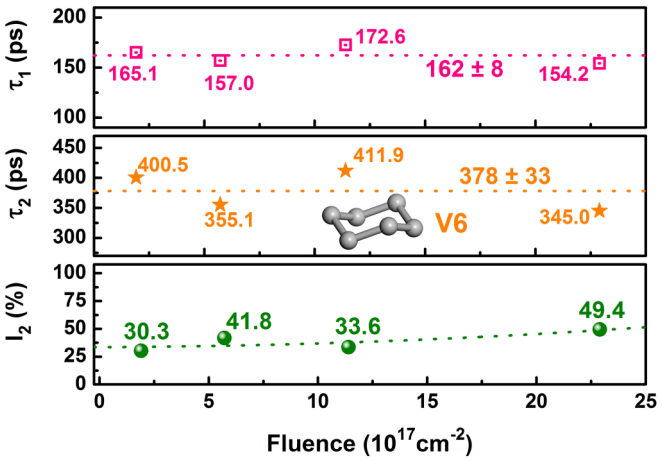

FIG. 5. Fitted results of τ_1 (pink square points), τ_2 (orange pentagrams), and I_2 (green balls) as functions of irradiation fluence. τ_1 and τ_2 are found to be independent of fluence. I_2 is associated positively with fluence. The dotted lines show the mean values of τ_1 as well as τ_2 while the correlation between I_2 and fluences of irradiation.

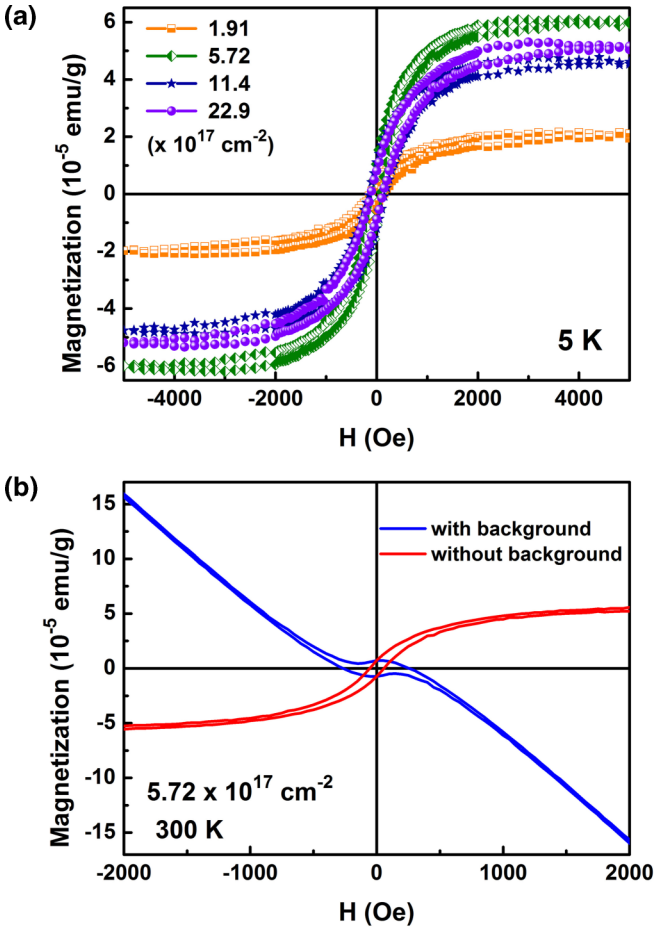

FIG. 6. (a) The magnetization as a function of magnetic field without the diamagnetic background. It is performed within a 5 kOe magnetic field at 5 K for irradiated and pristine silicon samples. (b) The *M-H* signals with and without the diamagnetic contribution in low magnetic field range for the sample with fluence of $5.72 \times 10^{17}\, n/\mathrm{cm}^2$ at $T = 300$ K.

samples [27]. After removing the diamagnetic background, the distinct hysteresis loops with FM features of irradiated silicon samples are revealed [Fig. 6(a)] and the saturation magnetization reaches 6×10^{-5} emu/g in the sample with the fluence of $5.72 \times 10^{17}\, n/\mathrm{cm}^2$. (All transition metal impurities cannot be detected by SIMS. The total concentration of the detection limits is $9 \times 10^{14}\,\mathrm{cm}^{-3}$, corresponding to the maximum saturation of 3.5×10^{-6} emu/g, if each impurity carries a moment of 1 μ_B. Therefore, the magnetism does not come from transition metals.) Even at 300 K, the saturation magnetization still remains about 5×10^{-5} emu/g shown in Fig. 6(b). Therefore, its transition temperature is above RT, which entails that the transition temperature limit set to the silicon-based diluted magnetic semiconductor will no longer be followed in defect-induced magnetism [28]. The absence of tiny parasitic or any secondary magnetic phase was confirmed by a smooth and featureless *M-T* curve [27]. Weak paramagnetism due to slight irradiation damage is revealed as both curves rise along with temperature dropping. Besides, the rise and fall of magnetization upon rising fluence is similar to the cases in ion implanted and neutron irradiated SiC [29,30], which again suggests that the existence of magnetization maximum is a feature of defect-induced magnetism.

The density of the local moments involved in ferromagnetism due to V6 is estimated to be $2.1 \times 10^{16}\,\mu_B\,\mathrm{cm}^{-3}$, so the V6 concentration should be $3.7 \times 10^{16}\,\mathrm{cm}^{-3}$ at the fluence of $5.72 \times 10^{17}\, n/\mathrm{cm}^2$. Referring to the previous result [17], the concentration of divacancy in SiC reckons as $1.4 \times 10^{17}\,\mathrm{cm}^{-3}$ at the fluence of $5.72 \times 10^{17}\, n/\mathrm{cm}^2$. Considering the neutron scattering cross section difference between silicon (2 barns) and carbon (5 barns) [20], the V6 concentration can thus be estimated to be $\sim 4.0 \times 10^{16}\,\mathrm{cm}^{-3}$, which is well consistent with that derived from the magnetic measurements based on the calculations above. Besides, the positive charge concentration with the level of $10^{14}\,\mathrm{cm}^{-3}$ is much less than the defect density with the level of $10^{16}\,\mathrm{cm}^{-3}$, so positively charged V6s can happen to be side by side with neutral V6s or even surrounded by them.

To further verify the magnetism in irradiated silicon and investigate its origin, we carried out electron spin resonance (ESR) and x-ray magnetic circular dichroism (XMCD) measurements. Figure 7(a) demonstrates the ESR spectra for both the pristine and $2.29 \times 10^{18}\, n/\mathrm{cm}^2$ irradiated silicon at 100 K. In the pristine silicon, no ESR signal was detected while the irradiated sample presented a clear resonance peak around 320 mT. Considering the diamagnetic background of silicon [27], this ESR signal is assigned to the FM resonance, which provides convincing evidence to support the ferromagnetism in silicon induced by neutron irradiation. (It should be noted that the capability of ESR to distinguish the type and the charge state of the defects is impeded due to the FM coupling.) The XMCD spectroscopy can establish a direct correlation between the ferromagnetism and the electrons/orbitals from a specific element [31,32]. As a robust element resolved technique, its signals are mainly collected from the contribution of the certain elements with partially occupied $3d$ or $4f$ subshells. Recently, in the study of d_0 magnetism, it is extended to

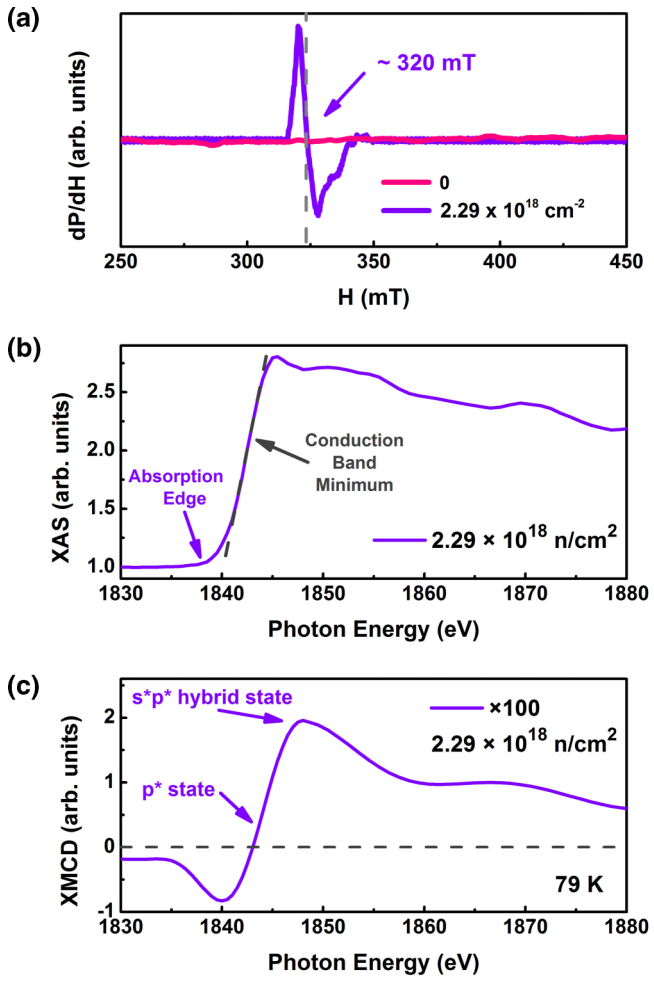

FIG. 7. (a) The ESR spectra of the pristine and $2.29 \times 10^{18}\, n/\mathrm{cm}^2$ irradiated samples at 100 K. (b) and (c) The XAS and XMCD spectra at the silicon K edge of the sample with the fluence of $2.29 \times 10^{18}\, n/\mathrm{cm}^2$ under a magnetic field of 5 kOe at 79 K.

include carbon or oxygen [15,16]. Figure 7(b) shows the typical x-ray absorption spectrum (XAS) at the silicon K edge of the $2.29 \times 10^{18}\, n/\mathrm{cm}^2$ sample at 79 K. The absorption edge at 1841 eV is corresponding to $3p$ electrons located near the conduction band minimum [33,34]. In the XMCD spectrum [Fig. 7(c)], a broad peak appears on the right of the conduction band minimum, where the bands could include both s^* and p^* states. So the ferromagnetism in irradiated silicon originates from spin-polarized electrons with $3s^*3p^*$ hybrid states. They are probably located at silicon atoms close to V6 sites according to the above prediction.

When the experimental data is in contrast with the theoretical prediction, we have to face the complication in the realistic situation. Due to the randomness during the process of V6 creation by the neutron irradiation, the ferromagnetism induced by V6 is not homogeneously distributed but probably exists in domains. The magnetization values obtained by dividing the magnetic moment by the total mass do not correspond to the expected intrinsic values. The built supercell is studied only for obtaining the relationship between magnetism and defects, and the structure of two supercells side by side is built to investigate the coupling, respectively. Both of them shall not be considered to represent a realistic distribution of defects.

We have so far investigated the magnetic properties of partially positive charged V6. The negatively charge state in silicon could be another option. Defect complexes may induce ferromagnetism in doped semiconductors such as Li-doped ZnO [35], V-doped SiC [36], Cu-doped SiC [37], Al-doped TiO_2 [38], as well as proton irradiated ZnO [39], SiC [40]. The control of the charge state plays a key role in this kind of works. The charged defect complexes in some wide band gap semiconductors like GaN [41] or SiC [42,43] also provide more opportunities. The defect complexes may induce ferromagnetism in two-dimensional materials like MoS_2 as well [44–46]. Besides, considering the study of the magnetism on the interface [47–49], it is worth investigating the magnetism of the interface between silicon substrates and the spontaneous/epitaxial oxide film.

In summary, we have theoretically predicted and then experimentally verified the spin order of V6 in silicon. First-principles calculations reveal dynamic stability of V6 and predict band splitting caused by spin polarization in the electronic structure of a neutral V6 but it has no net spin. It implies that any shift of its Fermi level can trigger the spin polarization. For positively charged $V6^+$, both s and p states of nearest-neighbor silicon atoms around it donate most of magnetic moments as the distortion brought by V6 is rather weak. The spin for half of the nearest-neighbor silicon atoms is up and the rest is down, while their magnitudes are different, similar to the ferrimagnetic order. The partially positively charged V6s could have the spin polarization at RT and obtain FM coupling. In irradiated silicon, magnetism is achieved as predicted. Its transition temperature is above RT. The saturation magnetization verifies the magnetic moments obtained in the calculations. The $3s^*3p^*$ hybrid states of slightly positively charged V6 are responsible for the observed magnetism. Our results will be helpful to understand the unique magnetic behavior of V6 affected by its charge due to its complexity in silicon and thus enlighten the study of defect complexes.

Y.L. would like to thank Dr. S. Prucnal of HZDR for the fruitful discussions and Dr. Y. L. Zhao of Peking University for the discussion of ESR. This work is financially supported by the Helmholtz Postdoc Programme (Initiative and Networking Fund, PD-146), Science Fund for Creative Research Groups of the National Natural Science Foundation of China (Grant No. 10821201), the National Natural Science Foundation of China (Grants No. 51532010, No. 51372056, and No. 51371192), Fundamental Research Funds for the Central University (Grants No. HIT.BRETIII.201220, No. HIT.NSRIF.2012045, and No. HIT.ICRST.2010008), International Science & Technology Cooperation Program of China (2012DFR50020), and the Program for New Century Excellent Talents in University (NCET-13-0174). Support by the Ion Beam Center (IBC) at HZDR is gratefully acknowledged. The Advanced Light Source is supported by the Director, Office of Science, Office of Basic Energy Sciences, of the U.S. Department of Energy under Contract No. DE-AC02-05CH11231.

[1] P. A. Packan, Science **285**, 2079 (1999).
[2] K. C. Pandey, A. Erbil, G. S. Cargill, R. F. Boehme, and D. Vanderbilt, Phys. Rev. Lett. **61**, 1282 (1988).
[3] M. Ramamoorthy and S. T. Pantelides, Phys. Rev. Lett. **76**, 4753 (1996).
[4] K. Saarinen, J. Nissila, H. Kauppinen, M. Hakala, M. J. Puska, P. Hautojarvi, and C. Corbel, Phys. Rev. Lett. **82**, 1883 (1999).
[5] P. M. Voyles, D. A. Muller, J. L. Grazul, P. H. Citrin, and H. J. L. Gossmann, Nature (London) **416**, 826 (2002).
[6] V. Ranki, J. Nissila, and K. Saarinen, Phys. Rev. Lett. **88**, 105506 (2002).
[7] M. Rummukainen, I. Makkonen, V. Ranki, M. J. Puska, K. Saarinen, and H. J. L. Gossmann, Phys. Rev. Lett. **94**, 165501 (2005).
[8] C. Y. Moon, W. J. Lee, and K. J. Chang, Nano Lett. **8**, 3086 (2008).
[9] S. K. Estreicher, J. L. Hastings, and P. A. Fedders, Appl. Phys. Lett. **70**, 432 (1997).
[10] J. L. Hastings, S. K. Estreicher, and P. A. Fedders, Phys. Rev. B **56**, 10215 (1997).
[11] D. J. Chadi, P. H. Citrin, C. H. Park, D. L. Adler, M. A. Marcus, and H. J. Gossmann, Phys. Rev. Lett. **79**, 4834 (1997).
[12] P. M. Voyles, D. J. Chadi, P. H. Citrin, D. A. Muller, J. L. Grazul, P. A. Northrup, and H. J. L. Gossmann, Phys. Rev. Lett. **91**, 125505 (2003).
[13] See Supplemental Material at http://link.aps.org/supplemental/10.1103/PhysRevB.94.195204 for calculation parameters.
[14] J. R. Weber, W. F. Koehl, J. B. Varley, A. Janotti, B. B. Buckley, C. G. Van de Walle, and D. D. Awschalom, P. Natl. Acad. Sci. **107**, 8513 (2010).
[15] H. Ohldag, T. Tyliszczak, R. Höhne, D. Spemann, P. Esquinazi, M. Ungureanu, and T. Butz, Phys. Rev. Lett. **98**, 187204 (2007).
[16] Y. T. Wang *et al.*, Sci. Rep. **5**, 8999 (2015).
[17] Y. Liu, G. Wang, S. C. Wang, J. H. Yang, L. A. Chen, X. B. Qin, B. Song, B. Y. Wang, and X. L. Chen, Phys. Rev. Lett. **106**, 087205 (2011).
[18] P. Dev, Y. Xue, and P. H. Zhang, Phys. Rev. Lett. **100**, 117204 (2008).
[19] See Supplemental Material at http://link.aps.org/supplemental/10.1103/PhysRevB.94.195204 for the details of materials, neutron irradiations, and all the measurements.
[20] http://www.oecd-nea.org/janisweb/book/neutrons.
[21] M. Alatalo, B. Barbiellini, M. Hakala, H. Kauppinen, T. Korhonen, M. J. Puska, K. Saarinen, P. Hautojärvi, and R. M. Nieminen, Phys. Rev. B **54**, 2397 (1996).
[22] K. Saarinen, T. Laine, S. Kuisma, J. Nissila, P. Hautojarvi, L. Dobrzynski, J. M. Baranowski, K. Pakula, R. Stepniewski, M. Wojdak, A. Wysmolek, T. Suski, M. Leszczynski, I. Grzegory, and S. Porowski, Phys. Rev. Lett. **79**, 3030 (1997).
[23] F. Tuomisto and I. Makkonen, Rev. Mod. Phys. **85**, 1583 (2013).
[24] J. Kansy, A. Hanc, L. Pająk, and D. Giebel, Phys. Status Solidi C **6**, 2326 (2009).
[25] Z. Wang, H. S. Leipner, R. Krause-Rehberg, V. Bodarenko, and H. Gu, Microelectron. Eng. **66**, 358 (2003).
[26] T. E. M. Staab, A. Sieck, M. Haugk, M. J. Puska, T. Frauenheim, and H. S. Leipner, Phys. Rev. B **65**, 115210 (2002).
[27] See Supplemental Material at http://link.aps.org/supplemental/10.1103/PhysRevB.94.195204 for the results of magnetic measurements in Figs. S1–S3.
[28] T. Dietl, H. Ohno, F. Matsukura, J. Cibert, and D. Ferrand, Science **287**, 1019 (2000).
[29] L. Li, S. Prucnal, S. D. Yao, K. Potzger, W. Anwand, A. Wagner, and S. Zhou, Appl. Phys. Lett. **98**, 222508 (2011).
[30] Y. Wang, Y. Liu, E. Wendler, R. Hubner, W. Anwand, G. Wang, X. Chen, W. Tong, Z. Yang, F. Munnik, G. Bukalis, X. Chen, S. Gemming, M. Helm, and S. Zhou, Phys. Rev. B **92**, 174409 (2015).
[31] G. Schutz, W. Wagner, W. Wilhelm, P. Kienle, R. Zeller, R. Frahm, and G. Materlik, Phys. Rev. Lett. **58**, 737 (1987).
[32] J. Stohr, H. A. Padmore, S. Anders, T. Stammler, and M. R. Scheinfein, Surf. Rev. Lett. **05**, 1297 (1998).
[33] J. C. Woicik, B. B. Pate, and P. Pianetta, Phys. Rev. B **39**, 8593 (1989).
[34] N. Nagashima, A. Nakano, K. Ogata, M. Tamura, K. Sugawara, and K. Hayakawa, Phys. Rev. B **48**, 18257 (1993).
[35] J. B. Yi, C. C. Lim, G. Z. Xing, H. M. Fan, L. H. Van, S. L. Huang, K. S. Yang, X. L. Huang, X. B. Qin, B. Y. Wang, T. Wu, L. Wang, H. T. Zhang, X. Y. Gao, T. Liu, A. T. S. Wee, Y. P. Feng, and J. Ding, Phys. Rev. Lett. **104**, 137201 (2010).
[36] S. Y. Zhuo, X. C. Liu, Z. Xiong, and W. S. Yan, Chin. Phys. B **21**, 067503 (2012).
[37] H. W. Zheng *et al.*, Appl. Phys. Lett. **102**, 142409 (2013).
[38] X. J. Wang *et al.*, Appl. Phys. Lett. **105**, 262402 (2014).
[39] M. Khalid and P. Esquinazi, Phys. Rev. B **85**, 134424 (2012).
[40] R. W. Zhou, X. C. Liu, H. J. Wang, W. B. Chen, F. Li, S. Y. Zhuo, and E. W. Shi, AIP Adv. **5**, 047146 (2015).
[41] P. Dev and P. H. Zhang, Phys. Rev. B **81**, 085207 (2010).
[42] L. Yu, H. Jin, D. H. Liu, Y. Dai, M. Guo, B. B. Huang, and Z. K. Zhang, Chem. Phys. Lett. **496**, 276 (2010).
[43] X. L. Lin and F. C. Pan, J. Supercond. Nov. Magn. **27**, 1513 (2014).
[44] H.-P. Komsa, J. Kotakoski, S. Kurasch, O. Lehtinen, U. Kaiser, and A. V. Krasheninnikov, Phys. Rev. Lett. **109**, 035503 (2012).
[45] H. Zheng, B. Yang, D. Wang, R. Han, X. Du, and Y. Yan, Appl. Phys. Lett. **104**, 132403 (2014).
[46] L. Cai *et al.*, J. Am. Chem. Soc. **137**, 2622 (2015).
[47] A. Brinkman *et al.*, Nat. Mater. **6**, 493 (2007).
[48] Ariando *et al.*, Nat. Commun. **2**, 188 (2011).
[49] F. Al Ma'Mari *et al.*, Nature (London) **524**, 69 (2015).